

Local structure study of the off-center displacement of Ti and Zr across the morphotropic phase boundary of $\text{PbZr}_{1-x}\text{Ti}_x\text{O}_3$ ($x=0.40, 0.47, 0.49, 0.55$)

D. Cao, I.-K. Jeong, R. H. Heffner, T. Darling, and J.-K. Lee
MS K764, Los Alamos National Laboratory, Los Alamos, New Mexico 87545, USA

F. Bridges
Physics Department, University of California, Santa Cruz, California 95064, USA

J.-S. Park and K.-S. Hong
School of Material Science and Engineering, Seoul National University, Seoul 151-742, Korea
 (Received 19 April 2004; revised manuscript received 7 July 2004; published 3 December 2004)

X-ray absorption fine structure (XAFS) experiments were carried out on a series of ferroelectric materials $\text{PbZr}_{1-x}\text{Ti}_x\text{O}_3$ (PZT) ($x=0.40, 0.47, 0.49, 0.55$) to study the local structure around Ti and Zr atoms in each sample. Based on the fact that PZT has a single phase in the morphotropic phase boundary (MPB) from the x-ray diffraction measurements, both extended XAFS (EXAFS) and x-ray absorption near-edge structure results suggest that at 3 K the orientation of the Ti off-center displacement in these materials changes gradually from the $[001]$ to $[111]$ direction (in pseudocubic notation) as the Ti concentration x decreases from 0.55 to 0.40. This is evidence for a continuous rotation of the local electrical polarization across the MPB region in PZT. The Zr K -edge EXAFS data suggest that at low temperature, the ZrO_6 octahedra in PZT are less distorted than indicated from the average structure for all samples, though a small Zr displacement relative to the O atoms may exist. This possible small Zr displacement is also much less than that found in density functional theory calculations. The ZrO_6 local structure hardly changes with Ti concentration across the MPB region. Finally, the XAFS data also show that the sizes of the ZrO_6 octahedra are larger than that of the TiO_6 octahedra which was also observed by experimental neutron pair distribution function analysis.

DOI: 10.1103/PhysRevB.70.224102

PACS number(s): 77.80.-e, 61.10.Ht, 77.84.Dy

I. INTRODUCTION

Ferroelectric materials with the perovskite structure have drawn considerable attention for many years. Among them, $\text{PbZr}_{1-x}\text{Ti}_x\text{O}_3$ (PZT) materials are particularly interesting due to their high piezoelectric response in the so-called “morphotropic phase boundary” (MPB) region. In the phase diagram established by Jaffe *et al.*,¹ there is a transition from tetragonal (T) to rhombohedral (R) phase when x is close to 0.5, and this phase transition has a very small Ti concentration dependence. Recently, synchrotron x-ray powder diffraction experiments done by Noheda *et al.* showed the existence of a monoclinic (M) phase between the tetragonal and rhombohedral phases.^{2,3} Bellaiche *et al.*, using a first-principles calculation, not only confirmed the theoretical existence of this monoclinic phase near the MPB region, but also provided an explanation for the large piezoelectricity in PZT.⁴ Further high-resolution x-ray powder diffraction measurements on poled PZT samples near the MPB region again showed that the monoclinic phase is crucial in understanding the origin of the large piezoelectric response in PZT.⁵

The crystal structure of cubic PZT (PZT above 800 K) is a perovskitelike structure, where the Pb atom is at each corner of the cubic lattice with Ti/Zr in the center. Oxygen atoms are at the face-centered positions. When the cubic lattice turns into the tetragonal phase as temperature decreases, both Pb and Ti/Zr will have an atomic displacement along the pseudocubic $[001]_c$ axis. (The subscript c indicates pseudocubic notation.) The O atom is also slightly displaced.

In the monoclinic phase, the displacements of the metal ions start to have a $[110]_c$ direction component. Figure 1 shows the lattice structure (eight unit cells) for a PZT sample in the tetragonal phase. Note that each $\text{Ti}(\text{Zr})\text{O}_6$ octahedron is corner shared with six other $\text{Ti}(\text{Zr})\text{O}_6$ octahedra. Since the Zr^{4+} and Ti^{4+} ions have different ionic radii, the random Zr and Ti positions in the lattice make the $\text{Ti}(\text{Zr})\text{O}_6$ octahedra slightly distorted. This distortion is not shown in Fig. 1.

In the tetragonal and rhombohedral phases of PZT, the electrical polarization \mathbf{P} is oriented along the $[001]_c$ and $[111]_c$ directions, respectively. Thus, the monoclinic phase may correspond to a continuous change in the direction of \mathbf{P} with Ti concentration x .² However, no direct experimental evidence has been found that the local polarization $\mathbf{P}_{\text{local}}$ has such a continuous rotation. Recent neutron pair distribution function (PDF) studies of the PZT materials near the MPB region suggest that the Ti off-center displacement is along $[001]_c$ in the T phase and along $[111]_c$ in the M and R phases, while the Zr displacement against the O atoms is very small.⁶ However, such results are not conclusive due to the fact that the Ti-O peaks and Zr-O peaks partially overlap each other in the PDF spectra. There are also contradictions between theoretical calculations and the PDF results concerning the Zr off-center displacement. Density functional theory (DFT) calculations using the local-density approximation (LDA) and the generalized-gradient approximation (GGA) suggest a rather large (0.2–0.3 Å) Zr off-center displacement,^{7–9} while the PDF measurements suggest that Zr is on center.⁶ Therefore, a more detailed experimental

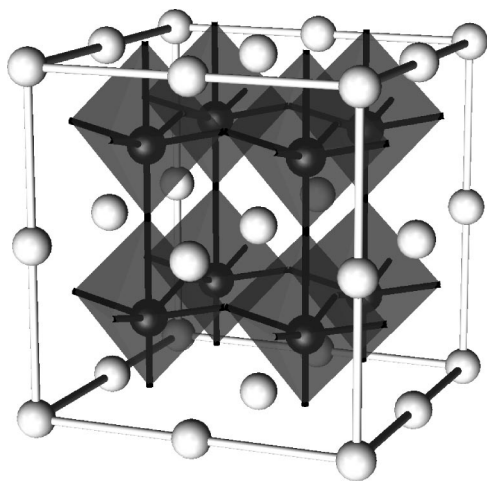


FIG. 1. Lattice structure (eight unit cells) of a PZT sample in the tetragonal phase. The white balls are Pb atoms, and the grey polyhedra are $\text{Ti}(\text{Zr})\text{O}_6$ octahedra. Oxygen atoms, which are not shown in the figure, are at the corners of each octahedron. $\text{Ti}(\text{Zr})$ atoms are the black balls inside each octahedron.

study of the local structure is needed to better understand the ferroelectric properties of PZT materials near the MPB region.

We used the x-ray absorption fine structure (XAFS) technique, a chemically sensitive local distortion detecting tool, to study the local structure of PZT materials with different phases. Four samples ($x=0.40, 0.47, 0.49$, and 0.55 ; here, x is the Ti concentration) were measured. The monoclinic phase of PZT exists at low temperature (20 K) for $0.46 \leq x \leq 0.51$.¹⁰ Therefore, as x decreases the lattice structure of the four samples at low temperatures changes from tetragonal ($x=0.55$) to monoclinic ($x=0.47, 0.49$) and then to rhombohedral ($x=0.40$). Since x-ray diffraction measurements conclude that PZT in the MPB region has a single phase, our XAFS results reported here clearly show that the TiO_6 local structure has a significant continuous change with x across the MPB region. Detailed data analysis and fitting further demonstrate that such a continuous change corresponds to a continuous rotation of the Ti local off-center displacement. This result provides evidence of a continuous rotation of $\mathbf{P}_{\text{local}}$ across the MPB region and suggests that the monoclinic phase indeed acts as a transitional bridge between the tetragonal and rhombohedral phases. A large low-temperature Debye-Waller factor was found for the Zr-O bond for all four PZT samples. This indicates that a small Zr off-center displacement (upper limit is ~ 0.07 Å) may exist. This value is clearly much less than that obtained from the DFT calculations and the refined average structure results. We also find that the ZrO_6 local structure is almost independent of Ti concentration. This possible small Zr off-center displacement may produce a non-negligible longitudinal (covalent) polarization and possibly contribute to the large piezoelectric response found near MPB region in PZT materials by providing additional polarization directions for their alignment under the electric field.^{11,12}

The experimental details are given in Sec. II, while Sec. III gives the analysis and discussion of the XAFS data. The conclusions are summarized in Sec. IV.

II. EXPERIMENTAL DETAILS

The experiments were carried out at beamline 10-2 of the Stanford Synchrotron Radiation Laboratory (SSRL) using Si $\langle 111 \rangle$ monochromator crystals and beamline 11-ID-D at the Advanced Photon Source (APS) using Si $\langle 220 \rangle$ monochromator crystals. XAFS data at the Ti K and Zr K edges were collected for the four PZT materials at temperatures below 10 K. A Ti metal foil was used as the reference when taking Ti K -edge data. The transmission XAFS data collection mode was used for both edges. The average structures of the PZT samples were obtained from neutron powder diffraction experiments.

All samples used in the XAFS experiments were powdered materials. $\text{Pb}(\text{Zr}_{1-x}\text{Ti}_x)\text{O}_3$ solid solution samples with $x=0.40, 0.47, 0.49$, and 0.55 were prepared using the mixed oxide method. Starting materials were reagent-grade PbO , ZrO_2 , and TiO_2 with a purity better than 99.9%. The powders were weighed and mixed by ball milling for 24 h with stabilized zirconia media and ethanol. After drying, the mixed powder was calcined at 850 °C for 2 h, and the calcined powder was ball milled for 24 h. The milled powder was then pressed into pellets at 1000 kg/cm² in a poly-vinyl alcohol (PVA) solution. After the burnout of the binder, the pellets were sintered at 1150 °C for 2 h. The sintering atmosphere was enriched in PbO vapor by using PbZrO_3 as a lead source to minimize the volatilization of lead. For the neutron scattering and XAFS experiments, the sintered samples were ground and sieved again. The sieved powders, smaller than 60 μm , were annealed at 600 °C for 2 h in air to remove the strain accumulated during the grinding. Finally, the powdered materials were reground and passed through a 400-mesh sieve. The resulting very fine powders were then brushed onto Scotch tape for XAFS measurements (powder size is ~ 5 – 10 μm on Scotch tape).

III. EXAFS DATA, ANALYSIS, AND DISCUSSION

A. Background information

The x-ray absorption coefficient μ is defined as $\mu = \mu_0(1 + \chi)$, where μ_0 is the background (embedded atom) function¹³ and χ is the XAFS function. In fact, χ is just the oscillation part of the absorption coefficient at energies above the absorption edge, coming from the interference of the outgoing and backscattered photoelectron waves. Theoretically χ is given by the following equation:

$$\begin{aligned} k\chi(k) &= \sum_i k\chi_i(k) \\ &= \text{Im} \sum_i A_i \int_0^\infty F_i(k, r) \frac{g_i(r_{0i}, r) e^{i[2kr + 2\delta_c(k) + \delta_i(k)]}}{r^2} dr, \end{aligned} \quad (1)$$

where χ_i is the extended XAFS (EXAFS) function for shell i , $F_i(k)$ is the backscattering amplitude of the photoelectron from neighbors i (it includes mean-free-path effects), $g_i(r_{0i}, r)$ is the pair distribution function for the atoms at a distance r_{0i} from the central atom—assumed to be Gaussian

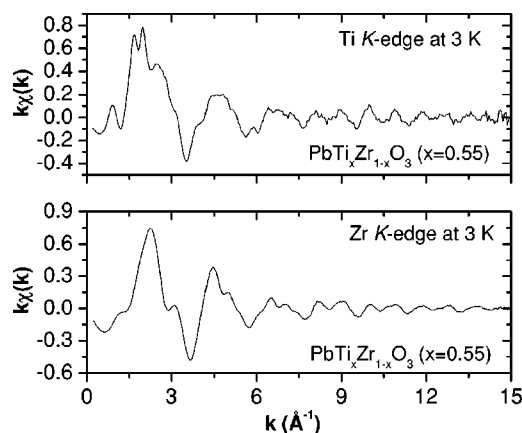


FIG. 2. A plot of the k -space XAFS data at Ti K and Zr K edges for the $x=0.55$ PZT sample at 3 K to show the quality of the data.

in most cases—and $\delta_c(k)$ and $\delta_i(k)$ are the phase shifts of the central and backscattered photoelectron waves. The amplitude factor A_i is given by

$$A_i = N_i S_0^2, \quad (2)$$

where N_i is the number of equivalent atoms in shell i and S_0^2 is the effective “amplitude reduction factor” that accounts primarily for many-body effects such as shake-up or shake-off, but also includes small corrections to the mean free path in the theoretical functions. In this equation, the photoelectron wave vector k is derived from $k = \sqrt{2m_e(E - E_0)}/\hbar$, where E_0 is the binding energy of the K - or L -shell electrons of the excited atom.

$k\chi(k)$ is also called the XAFS k -space data. Figure 2 presents the k -space data at the Ti and Zr K edges to show the quality of our XAFS data. Data at the Ti K edge are a little noisier, which is due to the low edge energy limiting the amount of material used in XAFS measurements and the strong background absorption of Pb and Zr.

The Fourier transform (FT) of $k\chi(k)$ is called r -space data, with peaks that correspond to different atomic shells. The position of each peak is shifted from its original pair distance due to the k dependence of the phase shifts $\delta_c(k)$ and $\delta_i(k)$. Based on the crystallographic information obtained from diffraction experiments, theoretical standards for each peak in r space are calculated using the FEFF8 code.¹⁴ We can therefore fit each peak in the experimental data using the calculated standards with a Gaussian pair distribution function. There are normally four parameters for each peak: σ (peak width), Δr (shift of peak position), A (peak amplitude), and ΔE_0 (shift of the electron binding energy). Higher cumulants C_3 and C_4 are also available in the fit but are not usually used.

B. Ti K -edge data analysis

The Ti K -edge r -space data at 3 K for the four PZT samples are shown in panel (a) of Fig. 3, where the structure from 1.0 to 2.0 Å corresponds to the nearest Ti-O bonds inside a TiO_6 octahedron. Since Ti in these materials has a significant off-center displacement, the large difference in

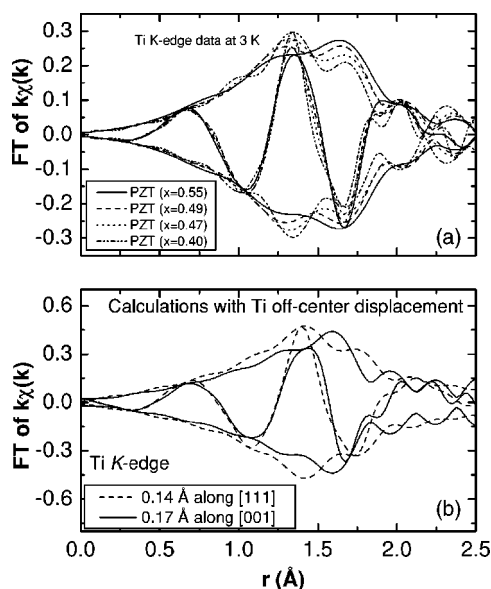


FIG. 3. (a) The Ti K -edge r -space data for the four PZT materials at 3 K. The Fourier transform range is 3.0–15 Å⁻¹, with 0.3 Å⁻¹ Gaussian broadening. The high-frequency curve inside the envelope is the real part of the FT (FT_R). The envelope is defined as $\pm\sqrt{\text{FT}_R^2 + \text{FT}_I^2}$ where FT_I is the imaginary part of the FT. (b): The theoretical calculations of Ti-O peaks for a TiO_6 octahedron with Ti off-center displacements along [001] and [111] directions, respectively, in a cubic SrTiO_3 lattice.

the Ti-O bond lengths leads to a double-peak structure for the nearest Ti-O peak instead of a single peak. Note that the amplitude of the first peak in the EXAFS data (~ 1.3 Å) decreases with Ti concentration x , while the amplitude of the second peak (~ 1.7 Å) increases with x . Such a continuous change in the r -space spectra indicates a continuous change in the TiO_6 local structure with x .

We used a perfect TiO_6 octahedron to simulate the off-center Ti displacement in PZT. Figure 3(b) shows theoretical calculations of the Ti-O peak with the Ti off-center displacement along the [001] and [111] directions. Since the shape of each TiO_6 octahedron in PZT changes slightly with Ti off-center displacement, such a simulation is only a qualitative estimation. As shown in Fig. 3(b), the simulated Ti displacements along both [001] and [111] directions lead to a double-peak structure for the Ti-O peak, as observed in our experiments. Note that the amplitudes of the peaks are different. The shape of the Ti-O peak in the calculations with [001] Ti displacement is very similar to that of the $x=0.55$ sample in Fig. 3(a), which suggests that the Ti off-center displacement in that sample is mainly along the $[001]_c$ direction. Similarly, the calculations indicate that the $x=0.40$ sample has a $[111]_c$ Ti displacement. The medium Ti-O peak amplitudes for the $x=0.47$ and 0.49 samples suggest that the orientation of the Ti displacements in these materials is between the $[001]_c$ and $[111]_c$ directions.

Fits to the Ti K -edge data were carried out for all samples. For a Ti displacement along the $[001]_c$ direction, there are one short, one long, and four medium Ti-O bonds. As the $[110]_c$ component of the Ti displacement increases (monoclinic phase), the four medium Ti-O bonds further

TABLE I. Obtained bond length for each Ti-O peak in the Ti *K*-edge *r*-space fit. The error is ~ 0.01 Å for the bond lengths obtained from EXAFS.

Sample	L_{1s} (Å)	L_{2s} (Å)	L_{2l} (Å)	L_{1l} (Å)	Mean error	Number of different peaks
PZT $x=0.55$	1.78	1.96	1.99	2.37	0.0225	3
PZT $x=0.49$	1.76	1.89	1.99	2.23	0.0386	4
PZT $x=0.47$	1.78	1.88	2.00	2.22	0.0551	4
PZT $x=0.40$	1.81	1.80	1.97	1.95	0.0547	2

break up into two long and two short bonds. If the $[110]_c$ component is large enough, the Ti displacement will point toward the $[111]_c$ direction and there will be three long and three short Ti-O bonds. We therefore fit the nearest Ti-O peak using four peaks: p_{1s} , p_{2s} , p_{2l} , and p_{1l} (the subscripts 1 and 2 represent the bond degeneracy, while *s* or *l* means the bond is shorter or longer; note that the bond lengths for p_{1s} and p_{2s} do not need to be the same). In the fit, A and ΔE_0 were fixed, while Δr was allowed to vary for each peak. The ratio of the peak amplitudes was also fixed in the ratio of the bond degeneracy for each peak. In order to reduce the number of free parameters in the fit, a simple model with same σ for all four peaks was applied. Other models were tried, in which the σ for each Ti-O bond yielded a slightly larger σ for the longer bonds, but the obtained bond lengths only varied by a very small amount (less than 0.01 Å) from that for the original simple model. Consequently, there are five free parameters in the fit. Since the fitting range is from 1.1 to 1.9 Å and the FT range is from 3.0 to 15.0 Å⁻¹, the maximum number of free parameters allowed is 8 (Ref. 15) which is more than what we actually used.

The fit quality can be quantified by the mean error between the data and the fit in the same unit as the data. The mean error is defined as¹⁶

$$\sqrt{\frac{\Delta_r^2 + \Delta_i^2}{\text{data}_r^2 + \text{data}_i^2}}, \quad (3)$$

where Δ_r and Δ_i are the difference between data and fit within the fit range for the real and imaginary parts of the Fourier transform, respectively, and data_r and data_i are the real and imaginary parts of the Fourier transform of the data within the fit range, respectively.

With all four Ti-O bond lengths extracted from the fit, we can then calculate the $[001]_c$ and $[110]_c$ components ($d_{[001]}$ and $d_{[110]}$, respectively) of the Ti off-center displacements and, therefore, determine the Ti local structure. The off-center displacements can be calculated as follows:

$$d_{[001]} = \frac{L_{1l}^2 - L_{1s}^2}{4l},$$

$$d_{[110]} = \frac{L_{2l}^2 - L_{2s}^2}{2\sqrt{2}l}. \quad (4)$$

Here l is the Ti-O bond length when Ti is in the center of a TiO₆ octahedron, while L_{1l} is the bond length for peak p_{1l}

and so on. Although it is possible that the TiO₆ octahedra can be slightly distorted due to some small O displacements, the above calculation is still a good approximation for the off-center displacements. The extracted bond lengths for each Ti-O peak are listed in Table I. Note that for data with a maximum k of 15 Å⁻¹, any adjacent peaks separated by less than 0.08 Å are normally considered as a single broadened peak as the resolution is not high enough to separate them. As shown in Table I, most obtained bond lengths are more than 0.08 Å apart. The exceptions are L_{2s} and L_{2l} for $x=0.55$, as well as L_{1s} and L_{2s} , L_{2l} , and L_{1l} for $x=0.40$. This is due to the fact that in $x=0.55$ PZT Ti has a $[001]_c$ displacement ($L_{2s} \approx L_{2l}$), while in $x=0.40$ PZT Ti has a $[111]_c$ displacement ($L_{1s} \approx L_{2s}$, $L_{2l} \approx L_{1l}$). In fact, taking the close distances to be equal does not change $d_{[100]}$ or $d_{[111]}$ significantly. Figure 4 shows the calculated $d_{[001]}$ and $d_{[110]}$ as a function of Ti concentration for all four samples. It is clear that $d_{[001]}$ increases as x increases, while $d_{[110]}$ decreases with x . Note that when $x=0.55$, $d_{[110]}$ is very small, which indicates a tetragonal local symmetry; when $x=0.40$, $d_{[110]} \approx \sqrt{2}d_{[001]}$, which indicates a rhombohedral local symmetry. Such results suggest that the Ti off-center displacement has a continuous rotation from the $[001]_c$ to the $[111]_c$ direction, as suggested by the average structure. Although

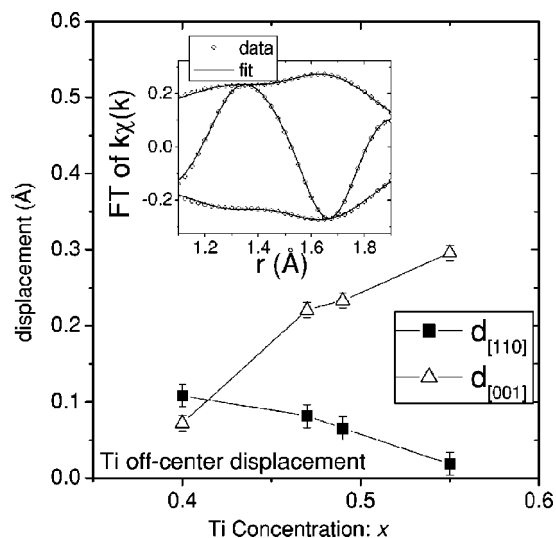


FIG. 4. Ti off-center displacement along both $[001]_c$ and $[110]_c$ directions extracted from the fit to the Ti *K*-edge data for all four PZT samples. The inset shows the fit result to the $x=0.55$ sample to give an example of the fit quality.

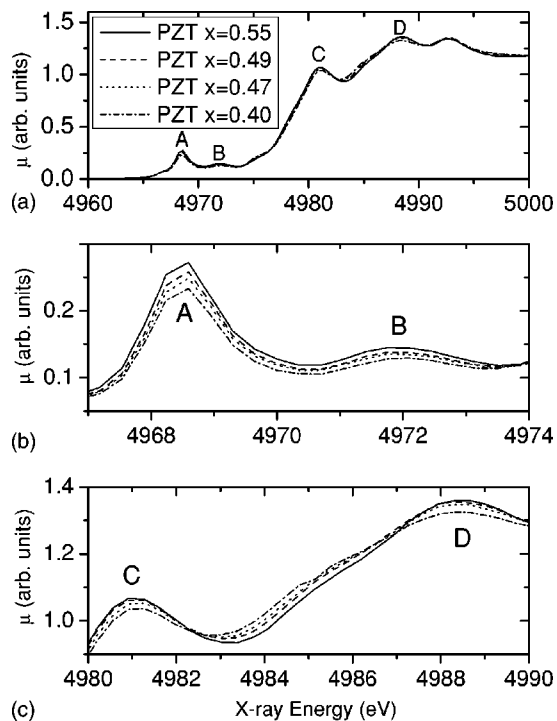


FIG. 5. Panel (a) shows the Ti K -edge XANES data for all samples at 3 K. Panels (b) and (c) show the detailed change of the near-edge structures near 4969, 4981, and 4988 eV. The same symbols are used in all panels. A Ti metal was used as a reference to adjust any possible edge shift caused by x-ray fluctuations. All edges were normalized with an edge-step height of 1 using a standard procedure.

the direction of the Ti local off-center displacement agrees with that obtained from the average structure, the magnitude of the displacement can be quite different from that in the average structure. For example, the neutron diffraction results suggest a ~ 0.37 Å Ti displacement for $x=0.55$ PZT at 10 K, while our XAFS data suggest a ~ 0.30 Å Ti displacement.

For the two samples in the monoclinic phase ($x=0.47$ and 0.49), we also fit the data with either a pure $[001]_c$ or $[111]_c$ Ti displacement to compare the fit quality with different models. For the $x=0.49$ sample, the mean errors [Eq. (3)] for the pure $[001]_c$ and $[111]_c$ models are 0.112 and 0.124, respectively, while for the $x=0.47$ sample, the mean errors are 0.131 and 0.128, respectively. By comparing these mean errors with those reported in Table I, we find that the fit with an intermediate Ti-displacement direction has the best fit quality, which further confirms the picture of a continuous rotation of the Ti off-center displacement.

In fact, what we obtain from the EXAFS results is the average change in the Ti local structure as a function of Ti concentration over the whole sample. Thus, taking the EXAFS data alone, it is impossible to distinguish a continuous rotation of Ti off-center displacement from a superposition of Ti displacements along the $[001]_c$ and $[111]_c$ directions in a mixed-phase PZT sample. However, the x-ray diffraction measurements done by Noheda *et al.* have clearly shown that the structural phase of PZT in the MPB region is

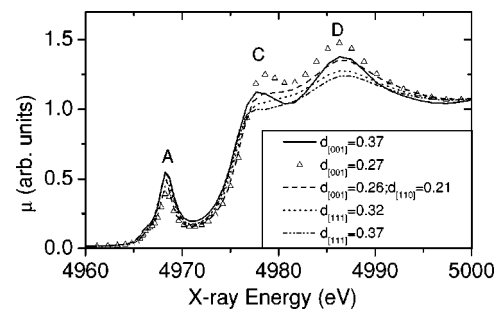


FIG. 6. Calculations of the XANES spectra using the FEFF8 code for PZT with different Ti off-center configurations.

monoclinic rather than mixed tetragonal and rhombohedral phases.^{2,3,10} Since it is unlikely that a PZT sample with a single structural phase has two completely different types of Ti off-center displacements, the possibility of the superposition of two different Ti displacements can, therefore, be excluded.

The x-ray absorption near-edge structure (XANES) data can also be used to study the TiO_6 local distortion. Figure 5 shows the Ti K -edge absorption spectra for the four PZT samples at 3 K, as well as the detailed changes of the peak structures near 4969 (peak A), 4981 (peak C), and 4988 eV (peak D). The main absorption edge, a result of $1s$ to $4p$ transitions, is near 4980 eV, while the peak structures near 4969 and 4972 eV (peak B) are pre-edge peaks caused by $1s$ to $3d$ transitions. Note as x decreases the amplitudes of peaks A, B, C, and D all become smaller. Such changes in the XANES spectra are likely related to changes in the Ti local structure. In order to demonstrate this, we carried out XANES calculations using the code FEFF8.¹⁷ First, the diffraction results for $x=0.55$ sample were used to calculate the Ti K -edge XANES spectra with tetragonal Ti local symmetry (Ti displaced along $[001]_c$, shown as a solid line in Fig. 6). We then allowed the Ti atom to move progressively toward the $[111]_c$ direction and observed the corresponding changes in the XANES spectra. The results are shown in Fig. 6. The FEFF8 calculations do a very good job of reproducing most of the main features of the XANES data, although the positions of the C and D peaks are slightly shifted. Note as the Ti off-center displacement rotates from the $[001]_c$ to the $[111]_c$ direction, the amplitudes of peaks C and D clearly decrease in Fig. 6. The amplitude of peak A also decreases with the amplitude of the overall Ti off-center displacement. Although a smaller $[001]_c$ Ti displacement can also decrease the amplitude of peak A, such a motion also makes peaks C and D much larger. From these calculations, we note that the amplitude of peak A is proportional to the overall displacement, $\sqrt{d_{[001]}^2 + d_{[111]}^2}$, while the amplitudes of peaks C and D decrease when $d_{[111]}$ gets larger. The XANES data are thus consistent with a continuous rotation of the Ti local displacement from the $[001]_c$ to the $[111]_c$ direction as x decreases. The calculations also indicate that the decrease of the amplitude of peak A comes from the decrease in the overall magnitude of the Ti displacement, which agrees with the fit results to the r -space data.

A previous XANES study of PZT materials by Ravel and Stern¹⁸ concluded that the Ti local structure is only weakly

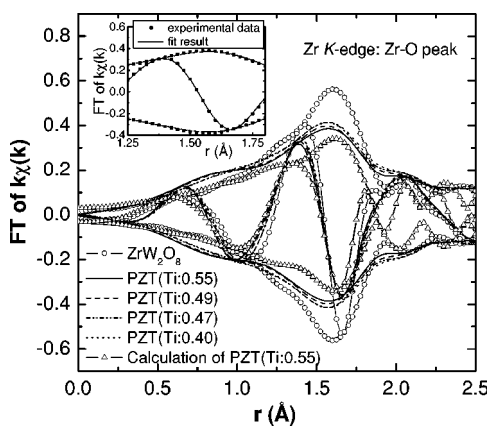


FIG. 7. Zr K -edge r -space data for all PZT samples at very low temperatures (3 K for $x=0.55$ and 0.49, 10 K for $x=0.47$ and 0.40). Theoretical calculations for $x=0.55$ average structure and ZrW_2O_8 experimental data at 20 K are also shown in the plot for comparison purposes. Only the nearest Zr-O peak is shown in this figure. The Fourier transform range is 3.0 – 15 \AA^{-1} , with 0.3 \AA^{-1} Gaussian broadening. The r -space data for the four samples are very close to each other, and the data of $x=0.40$ and 0.47 samples overlap at the peak near 1.6 \AA . The inset shows the $x=0.55$ PZT data at 3 K and the fit result within the fit range (1.25 – 1.80 \AA).

dependent on the crystallographic phase, based on the fact that changes in the pre-edge features of the Ti K -edge spectra with Ti concentration are relatively small. Our results agree with the small changes observed earlier in the pre-edge structure; however, our analysis shows that these small changes in the XANES spectra actually are consistent with a rotation of the Ti local displacement.

C. Zr K -edge data analysis

The Zr K -edge EXAFS r -space data at low temperatures (3 K for the $x=0.55$ and 0.49 samples and 10 K for the $x=0.47$ and 0.40 samples) are shown in Fig. 7. For comparison purposes, the theoretical standards for the Zr-O peak in the $x=0.55$ sample, as well as experimental EXAFS data for ZrW_2O_8 , are also plotted in the figure. Both the envelope and real parts of the experimental data are very similar for all PZT samples, which suggests that the Zr local structure hardly changes with x , though the Ti displacement changes significantly as shown earlier. The theoretical standard for $x=0.55$ was calculated based on the neutron diffraction results at 10 K in which the Zr is off center by 0.37 \AA . Note that the amplitude of the Zr-O peak in the theoretical standard is even smaller than that of the experimental data for the same sample. Since σ^2 was set to be zero in this calculation, the small amplitude of the calculated Zr-O peak compared to the data is simply due to the static Zr off-center displacement derived from the diffraction results. This indicates that the average Zr displacement obtained from diffraction measurements is overestimated. The ZrO_6 local structure in ZrW_2O_8 is well ordered at low temperatures, though a very small Zr off-center displacement (about 0.03 \AA) exists.¹⁹ The smaller amplitude of the Zr-O peak in the PZT samples suggests a more distorted ZrO_6 unit in these materials than found in ZrW_2O_8 .

Detailed fits were carried out for each sample in r space to obtain quantitative information about the ZrO_6 local distortion. Due to their overestimation of the Zr off-center displacement, the diffraction results for PZT cannot be used to generate the theoretical Zr-O standards for fitting the EXAFS data. We therefore used a well-ordered ZrO_6 octahedron to calculate a Zr-O theoretical standard and fit the Zr-O peak in each PZT material to obtain the Debye-Waller factor for the Zr-O bond at low temperatures. Single-peak fits (assuming Zr is on center) were carried out first (using a similar fitting procedure as for the Ti K -edge EXAFS data above). The inset of Fig. 7 shows an example of the fit quality for the $x=0.55$ sample. Fits for other samples have similar quality. The extracted σ^2 is $\sim 0.007 \text{ \AA}^2$ for the $x=0.55$ sample; this decreases slightly to 0.006 \AA^2 as x approaches 0.40. Since the zero-point motion of the Zr-O bond inside a ZrO_6 octahedron is only about 0.002 \AA^2 (Refs. 20 and 21), such a large low-temperature σ^2 for the Zr-O bond in PZT clearly indicates a static distortion of the ZrO_6 octahedra, which may come from a small Zr off-center displacement or randomly distorted ZrO_6 octahedra due to the random distribution of Ti and Zr atoms. However, EXAFS cannot tell the difference between these two possibilities. If there is a Zr off-center displacement, then the ZrO_6 unit will produce a small but non-negligible amount of “longitudinal polarization.” A rough estimation of the upper limit of such a Zr displacement is $\sim 0.07 \text{ \AA}$ ($\sqrt{0.007-0.002}$) for the $x=0.55$ sample ($\sim 0.06 \text{ \AA}$ for $x=0.40$). In the case that ZrO_6 octahedra are randomly distorted, the relative displacement of the O atoms may also move the center of the negative charge and produce some local polarization. Multipeak fits to the Zr-O peak, in analogy with the method used to analyze the Ti displacements discussed earlier, were also carried out. As the fit program tends to have the best fit when it fits the data with three peaks (peak amplitude ratio is 1:4:1), the Zr displacement is possibly along the $[001]_c$ direction (assuming the O stays roughly at its average position). The slight increase in σ^2 with x for the Zr-O peak possibly comes from the fact that more distortion is introduced in the ZrO_6 unit when the Ti concentration increases.

As suggested by recent neutron PDF studies for PZT, the Zr local structure is similar to that in pure $PbZrO_3$, which has almost no Zr displacement against the O atoms with only bending of the O-Zr-O bond.⁶ This then leads to a very small contribution, the so-called “longitudinal polarization.” In contrast, DFT calculations using LDA and GGA approximations suggest that Zr is displaced off center by 0.2 – 0.3 \AA , producing a Zr longitudinal polarization which is about 50% of the total polarization.^{7–9} Since the EXAFS technique is not sensitive to the transverse motion of the O atoms against the Zr, our results cannot tell whether there is a bending of the O-Zr-O bond or not. However, our EXAFS data do not rule out a small (0.06 – 0.07 \AA) Zr off-center displacement against the O atoms. This possible Zr displacement may contribute to the “longitudinal polarization” of PZT, though its amount is much smaller than that predicted by DFT calculations. Because the PDF technique has difficulty separating the Zr-O peak from its neighboring Ti-O peak(s) and the Rietveld average structure refinement cannot distinguish the Ti and Zr sites in PZT, these XAFS measurements provide important

new experimental results regarding the local structure of the ZrO_6 unit. Such results will certainly help theorists build a better picture of the Zr local displacement.

As measured in the PDF experiments, the average Zr-O bond length (~ 2.1 Å) is slightly larger than that of the Ti-O bond (1.85 – 1.9 Å).⁶ The DFT calculations also give different Zr-O and Ti-O bond lengths.^{7–9} From our XAFS data analysis, the obtained average Zr-O bond length is 2.07 – 2.08 Å (the error is about 0.01 Å) for all PZT samples, which has no obvious x dependence. This agrees very well with the PDF results. From the discussion above in Sec. III B, the Ti-O average bond length is about 2.00 Å for $x=0.55$, decreasing to ~ 1.89 Å for $x=0.40$. The average Ti-O bond length obtained from the PDF experiment is slightly smaller than that extracted from our EXAFS data. This is possibly due to the splitting of the Ti-O peak and the overlapping of Ti-O and Zr-O peaks in PDF spectra. However, both techniques agree that the size of the ZrO_6 octahedra are larger than that of the TiO_6 octahedra.

IV. CONCLUSION

The Ti K -edge XAFS spectra clearly show a continuous change in the Ti local structure of PZT across the MPB region. Detailed analysis further shows that the Ti local off-center displacement rotates continuously from the $[001]_c$ to $[111]_c$ directions as x decreases from 0.55 to 0.40 . Such a result suggests that the local polarization of the Ti sites fol-

lows the overall polarization, which confirms the possibility that the monoclinic phase acts as a transitional bridge between the tetragonal and rhombohedral phases.

A large low-temperature Debye-Waller factor was found for the Zr-O bond for all PZT samples. This gives the possibility that Zr may have a small off-center displacement relative to the O atoms. Such a result does not quite agree with PDF experiments in which almost no Zr displacement against the O atoms was found, but the disagreement is small. However, our results seriously disagree with the DFT calculations, as do the PDF results. The XAFS data suggest that the Zr sites might produce a non-negligible amount of longitudinal polarization which may also contribute to the high piezoelectric response in MPB region for PZT. Different average sizes for TiO_6 and Zr_6 octahedra are also found from our XAFS analysis. This result agrees well with the PDF experiments and the DFT calculations.

ACKNOWLEDGMENTS

Works by D.C., I.K.J., R.H.H., T.D., and J.K.L. were carried out under the auspices of the U.S. Department of Energy, Office of Science. Part of the experiments were performed at SSRL, which is operated by the DOE, Division of Chemical Sciences, and by the NIH, Biomedical Resource Technology Program, Division of Research Resources. Part of the experiments were performed at APS, which is funded by the DOE, Office of Sciences, Office of Basic Energy Sciences.

-
- ¹B. Jaffe, W. R. Cook, and H. Jaffe, *Piezoelectric Ceramics* (Academic Press, London, 1971).
- ²B. Noheda, D. E. Cox, G. Shirane, J. A. Gonzalo, L. E. Cross, and S.-E. Park, *Appl. Phys. Lett.* **74**, 2059 (1999).
- ³B. Noheda, J. A. Gonzalo, L. E. Cross, R. Guo, S.-E. Park, D. E. Cox, and G. Shirane, *Phys. Rev. B* **61**, 8687 (2000).
- ⁴L. Bellaiche, A. Garcia, and D. Vanderbilt, *Phys. Rev. Lett.* **84**, 5427 (2000).
- ⁵R. Guo, L. E. Cross, S.-E. Park, B. Noheda, D. E. Cox, and G. Shirane, *Phys. Rev. Lett.* **84**, 5423 (2000).
- ⁶W. Dmowski, T. Egami, L. Farber, and P. K. Davies, in *Fundamental Physics of Ferroelectrics 2001*, edited by Henry Krakauer, AIP Conf. Proc.No. 582 (AIP, Melville, NY, 2001), p. 33.
- ⁷V. R. Cooper, I. Grinberg, N. R. Martin, and A. M. Rappe, in *Fundamental Physics of Ferroelectrics 2002*, edited by Ronald E. Cohen, AIP Conf. Proc.No. 626 (AIP, Melville, NY, 2002), p. 26.
- ⁸I. Grinberg, V. R. Cooper, and A. M. Rappe, *Nature (London)* **419**, 909 (2002).
- ⁹J. A. Rodriguez, A. Etxebarria, L. González, and A. Maiti, *J. Chem. Phys.* **117**, 2669 (2002).
- ¹⁰B. Noheda, D. E. Cox, G. Shirane, R. Guo, and L. E. Cross, *Phys. Rev. B* **63**, 014103 (2000).
- ¹¹V. A. Isupov, *Sov. Phys. Solid State* **10**, 989 (1968).
- ¹²W. Heywang, *Z. Angew. Phys.* **19**, 473 (1965).
- ¹³J. J. Rehr, C. H. Booth, F. Bridges, and S. I. Zabinsky, *Phys. Rev. B* **49**, 12 347 (1994).
- ¹⁴S. I. Zabinsky, J. J. Rehr, A. Ankudinov, R. C. Albers, and M. J. Eller, *Phys. Rev. B* **52**, 2995 (1995).
- ¹⁵E. A. Stern, *Phys. Rev. B* **48**, 9825 (1993).
- ¹⁶One can find details in the RSXAP EXAFS analysis package at “<http://lise.lbl.gov/RSXAP/index.html>”
- ¹⁷A. L. Ankudinov, B. Ravel, J. J. Rehr, and S. D. Conradson, *Phys. Rev. B* **58**, 7565 (1998).
- ¹⁸B. Ravel and E. A. Stern, *Physica B* **208-209**, 316 (1995).
- ¹⁹J. D. Jorgensen, Z. Hu, S. Teslic, D. N. Argyriou, S. Short, J. S. O. Evans, and A. W. Sleight, *Phys. Rev. B* **59**, 215 (1999).
- ²⁰D. Cao, F. Bridges, G. R. Kowach, and A. P. Ramirez, *Phys. Rev. Lett.* **89**, 215902 (2002).
- ²¹D. Cao, F. Bridges, G. R. Kowach, and A. P. Ramirez, *Phys. Rev. B* **68**, 014303 (2003).